ISSN 1063-7710, Acoustical Physics, 2024, Vol. 70, No. 4, pp. 641–658. © Pleiades Publishing, Ltd., 2024.

OCEAN ACOUSTICS. HYDROACOUSTICS

On the Average Field Intensity and Individual Modes of a Low-Frequency Sound Signal in a Shallow Waveguide with a Statistically Rough Bottom Boundary

O. E. Gulin[a, *], **I. O. Yaroshchuk**[a], **and R. A. Korotchenko**[a]

[a] *Il'ichev Pacific Oceanological Institute, Far Eastern Branch, Russian Academy of Sciences, Vladivostok, 690041 Russia*

**e-mail: gulinoe@poi.dvo.ru*

Received March 28, 2023; revised June 14, 2024; accepted June 19, 2024

Abstract—For a low-frequency sound signal propagating in a horizontally inhomogeneous waveguide in shallow water, the influence of a fluctuating interface between the water layer and fluid bottom sediments was studied based on statistical modeling using the cross-sectional method. The modeling was carried out for hydrological conditions in many situations corresponding to the shallow shelf zones of the Russian Arctic seas. A specific feature of these water areas is the presence of an almost homogeneous water layer on poorly consolidated bottom sediments with various characteristics, including a high degree of gas saturation. The dependence of the average intensity of the sound signal and its individual modes on the parameters of the problem has been studied: the characteristic scale of fluctuations of the interface and impedance of this interface, which determines its penetrable properties. It is shown that the influence of bathymetric fluctuations on the average intensity of acoustic modes has its own characteristics versus the influence of random volumetric inhomogeneities of the sound speed in the water layer and sediments, established earlier. Thus, bottom roughness of a relatively small scale leads, on average, to increased attenuation of a sound signal when propagating in a waveguide, and this can occur at relatively short distances from the source. An increase in the reflectivity of a rough bottom boundary weakens the effect of increased sound attenuation so that for typical values of sound speed in the bottom, attenuation at distances of 10–20 km from the source differs little from that for an undisturbed horizontal boundary.

Keywords: horizontally inhomogeneous random shallow water, statistically rough boundary, average field intensity and its fluctuations, cross-sectional method, local modes, statistical modeling

DOI: 10.1134/S1063771024602437

1. INTRODUCTION

Low-frequency acoustic signals propagating in a shallow-water waveguide are subjected to the influence of all sorts of random inhomogeneities, which often greatly alter the pattern of average propagation losses (behavior of average intensity) and other sound field characteristics. This article considers the influence of a randomly rough bottom surface. A large number of works are devoted to sound scattering by rough surfaces. Among the pioneering articles, it is necessary to mention [1–3], as well as early reviews [4–6], where one can find numerous additional references to the literature on the topic. A modern representative review can be found in [7]. The above-mentioned works present the main approaches to approximate theoretical analysis and obtain results on individual aspects of the problem. The most common analytical methods are perturbation theory, Kirchhoff's method, and the integral equation method. Early theoretical studies treated surface and volume scattering as completely different problems. However, in shallow-water acoustics this often does not meet practical needs. Thus, it is difficult to distinguish, using experimental methods, scattering by irregularities of the seabed in a waveguide from scattering by volumetric inhomogeneities of bottom sediments. For this reason, recently an increasing number of authors have been studying these two types of sound scattering together [8, 9].

To calculate the scattered field from both volumetric and surface inhomogeneities of the medium, the vast majority of authors used the ray method, the parabolic equation method (PEM) and the mode approach. As is known, the ray method is applicable only for high-frequency fields, and is accompanied by computational difficulties at the points of ray turning and on caustics. The PEM also experiences difficulties in describing the sound focusing regions in the waveguide [10], and in addition, within the framework of the traditional form of the PEM for waveguides with rough boundaries, strict consideration of boundary conditions is problematic [11–13]. We will point out articles [14–16] that are close in their formulation of the problem to our study for mode waveguides in the low-frequency range. Thus, in [15], the Kirchhoff method for the Green's function, first developed in works [1–3, 14], was used in the form of a mode representation for layered-inhomogeneous waveguides with horizontal boundaries, and scattering by the roughness of the boundaries was calculated using the perturbation method. For short sound propagation distances, correlation functions and field coherence in the vertical and horizontal directions were calculated. In [16], a variation of the local mode approach proposed earlier in [17] and involving convolution along the horizontal coordinate of the adiabatic solution for a 2D waveguide with the mode coupling coefficients was applied to calculate scattering on random bottom roughness. The authors of the article considered the scattering of broadband signals for a fixed distance using the Fourier method in the time domain. However, the features of the decrease in average intensity and the behavior of other statistical characteristics of the sound field in waveguides with losses and a fluctuating water–bottom sediment interface are not considered in the above-mentioned literature. The present study is based on statistical modeling [18–21] of the average sound intensity, as well as intensity fluctuations (scintillations). The authors focus not so much on changes in the law of decay in intensity, which describes energy losses during signal propagation in a randomly inhomogeneous medium of a shallow water, which is the subject of articles [22–24], but on the specific features of the transformation of the intensity of individual modes that form the sound field. This sheds additional light on both intermodal coupling and signal behavior. In addition, statistical effects are analyzed for two types of impedance water–bottom sediment interfaces, when there is a strong acoustic energy transmission [24, 25], and, conversely, when there is a strong reflection from the interface. Using statistical modeling, the problem is solved for individual random realizations of the waveguide bathymetry from a representative ensemble of sampling with subsequent averaging. Calculations in each sampling are carried out on the basis of the universal local mode approach developed in [26–30]. In this approach, the distance-dependent mode amplitudes are sought by reformulating the original boundary value problem for the acoustic equations into equivalent first-order causal equations [26, 27], using the embedding method (also known as the parameter differentiation method or the Riccati equation method). The given causal equations allow an explicit representation of the solution in terms of backscattering coefficients, which significantly simplifies further calculations in the forward scattering approximation, or one-way propagation (OWP), when the contribution of the backscattered field in the waveguide is ignored.

2. FORMULATION OF THE PROBLEM

In a two-dimensionally inhomogeneous shallow-water waveguide with an roughboundary H, separating the water layer and fluid bottom sediments, the sound field with frequency ω is described by linear acoustic equations for the functions of the sound pressure and particle velocity components. On the sea surface and bottom H (or any horizon of the liquid sediment half-space) suitable boundary conditions are formulated. Let us consider an axially symmetric formulation of the problem for a monochromatic signal, omitting the time factor $e^{-i\omega t}$. In a medium with variable density, the acoustic equations are reduced to a single equation for sound pressure p of the following type [12]:

$$\begin{gathered}\rho r^{-1}\frac{\partial}{\partial r}\left(r\rho^{-1}\frac{\partial p(r,z)}{\partial r}\right)+\rho\frac{\partial}{\partial z}\left(\rho^{-1}\frac{\partial p(r,z)}{\partial z}\right)\\ +\frac{\omega^2}{c^2}p(r,z)=-\frac{\delta(r)\delta(z-z_0)}{2\pi r},\end{gathered}\tag{1}$$

in which (r, z) are the coordinates of the cylindrical system, the point source of radiation is located at $r = 0$, $z = z_0$; $c = c(r, z)$ is the sound speed; $\rho = \rho(r, z)$ is the density. Let us assume that on the free surface the boundary condition $p(r, 0) = 0$, and the condition at the bottom interface corresponds to the continuity of pressure and the velocity component normal to the roughinterface $H(r)$. It also implies that the radiation conditions are met at $z, r \to \infty$. As is known [11, 12], the pressure field $p(r, z)$ for (1) in the cross-sectional method can be sought using expansion in local modes of a horizontally inhomogeneous waveguide:

$$\begin{gathered}p(r,z)=\sum_{m=1}^{M}G_m(r)\,\varphi_m(r,z),\\ \frac{\partial^2}{\partial z^2}\varphi_m(r,z)+\left[k^2-\kappa_m^2(r)\right]\varphi_m(r,z)=0\,.\end{gathered}\tag{2}$$

In (2) $k = \omega cs(r, z)$, $\kappa_m(r)$ are the eigenvalues, and φ_m are the eigenfunctions of the Sturm–Liouville problem ($m = 1, 2,\ldots, M$), which on the surface and on the ocean floor satisfy the following boundary conditions: $\varphi_m(r,0) = 0$, $\varphi_m(r, H) + g_m(r)\varphi'_m(r, H) = 0$ ($\varphi'_m(r, H) = (\partial\varphi_m(r, z)/\partial z)|_{z = H}$). In the last condition, $g_m(r)$ characterizes the impedance of a penetrable bottom, and the rough boundary $H(r)$ is set as a random function, as a result of which problem (1)–(2) becomes stochastic. Obviously, the eigenfunctions and eigenvalues, as well as the waveguide modes $G_m(r)\varphi_m(r, z)$, will be random functions of r. The condition of a water–fluid sediment interface $H(r)$ corresponds to the continuity of pressure and the vertical component of the mode velocity when the boundary is crossed: $\varphi_m(r, H - 0) = \varphi_m(r, H + 0)$, $\varphi'_m(r, H - 0)/\rho(r, H - 0) = \varphi'_m(r, H + 0)/\rho(r, H + 0)$. At the same time, for the total acoustic field, in addition to Eq. (1), the condition of continuity of the velocity component normal to the boundary must be satisfied.

We further assume that the irregular part of the waveguide with random bathymetry is concentrated in an arbitrary horizontal region to the right of the sound source $0 < L < r < L_0$, and random fluctuations in bathymetry have relatively small amplitude and characteristic scales exceeding the wavelength of sound. In such a situation, the backscattered field of the modes in the waveguide is small and can be neglected with sufficient accuracy. In this approximation of OWP (or forward scattering), we use the following form of solution (3) for the mode amplitude vector $\mathbf{G}(r) = \{G_m(r)\}^T$, $m = 1,..M$, in closed form, following from the embedding equations. For the readers' convenience, Appendix A gives the derivation of the embedding equations and, as a special case, Eq. (3) for the mode amplitudes in the absence of backscattering (see also [29, 30]):

$$\begin{gathered}\mathbf{G}(r) = G(r;L)\mathbf{b}(L), \\ \frac{\partial}{\partial L}G(r;L) = G(r;L)C(L),\ \ G(r;L)\big|_{L=r} = E, \\ C(L) = -i\kappa(L) + \kappa'(L)/(2\kappa(L)) \\ +[V(L) - \kappa^{-1}(L)V^T(L)\kappa(L)]/2,\end{gathered} \tag{3}$$

where L is a variable parameter of the position of the boundary of the irregular medium, $G(r;\,L) \equiv G(r)$ is a square matrix of size $M \times M$ to be determined, $\mathbf{b}(L)$ is the column vector of the amplitudes of incident modes in the section $r = L$ of an irregular environment with M elements $b_m(L) = \varphi_m(0,\,z_0)\kappa_m^{-1/2}(L)\exp[i\kappa_m(L)L]$, $\kappa(r)$ is the diagonal matrix $\kappa_m(r)$, $\kappa'(r)$ is the diagonal matrix of derivatives $\kappa_m(r)$, and E is an identity matrix. Also, in (3) $V(r)$, a matrix with elements $V_{mn}(r) = \int_0^\infty \frac{\varphi_m(r,z)}{\rho(r,z)}\frac{\partial\varphi_n(r,z)}{\partial r}dz$, $V^T(r)$ is a transposed matrix with elements V_{nm}. Bearing in mind the wave zone $\kappa_m r \gg 1$ for the study, in expressions (3), a transition was made from cylindrical to exponential functions, and instead of expansion (2) for $p(r,\,z)$ we consider $p(r,\ z) = Ar^{-1/2}\sum_{m=1}^{M} G_m(r)\varphi_m(r,z)$, $A = i[8\pi i]^{-1/2}$. The representation of solution (3) may vary depending on the specific objectives of the study. From the viewpoint of direct calculations performed further in this study, the matrix notation of solution (3) is preferable. It was previously used in [23, 25, 29]. Note that the solution to Eq. (3) in transposed form is a matricant that allows exponential representation of the solution (in terms of a matrix exponent) if at each step of the computational procedure $C(L)$ is approximated along the propagation path by a constant matrix (then over the entire interval the matricant is represented by the product of the exponentials, see Appendix A).

Matrix $V(r)$ and the transposed matrix $V^T(r)$ describe intermode coupling due to horizontal variations caused by random roughness of the bottom boundary H. It is important to note that in order to satisfy the boundary condition of continuity of the normal to the boundary $H(r)$ of the velocity component required for Eq. (1), solution (3) must include the transposed matrix $V^T(r) = -V(r) - \int_0^\infty \varphi_m(r,z)\varphi_n(r,z)\frac{\partial}{\partial r}\left(\frac{1}{\rho(r,z)}\right)dz$ [11, 29].

Within the cross-sectional method for modes, this matrix ensures correct account for continuous (piecewise continuous) variations of the interface $H(r)$ with a jumplike change in density when the boundary is crossed. This makes it possible to satisfy the reciprocity principle and the energy conservation law in the acoustic field [11]. Thus, for waveguides with variable density and an irregular bottom boundary studied in here, the known approximate methods, adiabatic ($V_{mn} = 0$), the parabolic equation and the WKB equation in the traditional form do not strictly describe the boundary condition on the nonhorizontal interface $H(r)$. These approximations work well if the density of the medium and interfaces with different densities on either side of the interface do not change in the horizontal direction, and the waveguide contains, e.g., only volumetric inhomogeneities in the sound speed. Then the matrix $V(r)$ becomes skew-symmetric: $V_{mn}(r) = -V_{nm}(r)$, $V_{nn} = 0$, and expression in (3) is simplified [21–23, 25].

Calculating the pressure field $p(r,\,z)$ using Eqs. (2), (3) for each random realization $H(r)$ from the ensemble N implementations, we obtain the change in the average intensity, or the average loss function during the propagation of sound along the path in a randomly inhomogeneous waveguide in the form

$$\begin{gathered}\langle I\rangle = \left\langle |p|^2\right\rangle = r^{-1}\sum_{m=1}^{M}\left\langle |G_m|^2|\varphi_m|^2\right\rangle \\ +\ r^{-1}\sum_{(m\neq n)}\left\langle G_m G_n^*\left(\varphi_m\,\varphi_n^*\right)\right\rangle,\end{gathered} \tag{4}$$

where M is the maximum mode number taken into account in the calculations, and angle brackets mean statistical averaging, which is replaced in the calculations by the algebraic formula $\langle I\rangle = \frac{1}{N}\sum_{k=1}^{N} I_k$; I_k is intensity of the sound signal in the k-realization of the statistical ensemble. The first sum of modes in (4) represents incoherent terms and describes the averaged (over the scale of spatial interference) law of intensity decay in the waveguide. The second sum of coherent terms describes the wave interference structure of the sound field, which is superimposed on the smooth averaged law of decay. Other interesting statistical characteristics of intensity can also be calculated using well-known formulas. For example, an important indicator of relative fluctuations in sound intensity in

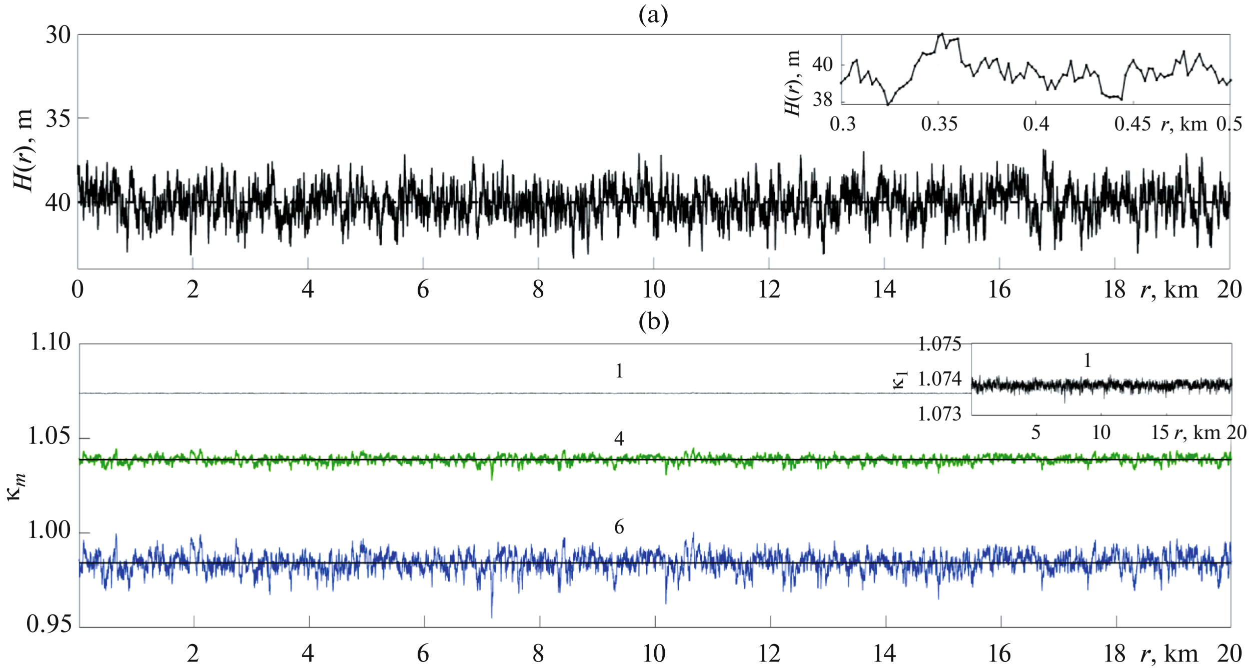

Fig. 1. Illustration of stochastic waveguide model. Penetrable boundary. (a) Example of random sampling of fluctuations $\delta h(r)$ of water–bottom sediment interface, $L_h = 20$ m; (b) arbitrary random realization of real part of eigenvalues $\kappa_m(r)$ of numbers $m = 1, 4, 6$.

a randomly inhomogeneous waveguide is the scintillation index S^2, where $S = [\langle I^2\rangle - \langle I\rangle^2]^{1/2}/\langle I\rangle$ [23, 25, 31].

3. SHALLOW-WATER STOCHASTIC WAVEGUIDE MODEL

For numerical analysis, reference was made to the values of parameters characteristic of the shelf zones of a number of Arctic seas, in particular, the Kara Sea [32, 33]. A shallow-water waveguide was considered in which a tonal sound signal with a frequency of 250 Hz (wavelength $\lambda = 6$ m) propagates. The waveguide has an average depth of $\langle H(r)\rangle = 40$ m, horizontal surface, and a randomly rough bottom. In the water layer $0 \le z < H(r)$ there are uniform sound speed profiles $c = 1460$ m/s and density $\rho = 1.023$ g/cm^3. The bottom $z \ge H(r)$ is a fluid absorbing half-space of unconsolidated sediments with a refractive index at the water–bottom interface $n = (c/c_1)(1 + i\beta_1)$. In bottom sediments, following the measurement data given in [33], we set the impedance in terms of density, $\rho_1 = 1.85$ g/cm^3, absorption $\beta_1 = 0.02$ (≈ 1 dB/λ) and sound speed c_1. Random irregularities of the water–sediment interface $\delta h(r)$, $H(r) = \langle H\rangle + \delta h(r)$ (Fig. 1a) we assume to be a Gaussian random process with an exponential correlation function: $B_h(r_2 - r_1) = \sigma_h^2 \exp(-|r_2 - r_1|/L_h)$. The intensity of fluctuations was given by the value $\sigma_h^2 = \langle(\delta h)^2\rangle = 1$ m^2 [15, 31], $\sigma_h \ll H$. The most important parameter L_h is the characteristic scale of change in bathymetry $H(r)$. The aim of this work is to study the influence of fluctuations $\delta h(r)$ small scale, but such that the statistical scale L_h exceeded the wavelength of sound and the amplitude σ_h ($L_h \gg \sigma_h$). In such a situation, as calculations show, the magnitude of the backscattered field is negligibly small, in addition, the requirements for sufficiently fast convergence of the mode series (2) of the cross-sectional method are not violated [11].

At a constant sound speed in the water layer and bottom sediments, the impedance function $g_m(r)$ in the boundary condition to Eqs. (2) is determined by its local values in the cross sections of the Pekeris comparison waveguides: $g_m(r) = i\rho_1(r)\rho^{-1}\left[k^2n^2 - \kappa_m^2(r)\right]^{-1/2}$, or if $c = c(z)$, any other comparison waveguides. In numerical modeling, when averaging (4), an ensemble of $N = 10^3$ samplings was considered to obtain a reliable statistical result. Figure 1 shows the fluctuations of the bottom boundary and eigenvalues $\kappa_m(r)$ of a randomly inhomogeneous waveguide that are perturbed by these fluctuations along the path. The numbers on the graphs in Fig. 1b correspond to the numbers of the eigenvalues.

4. STATISTICAL ANALYSIS OF THE BEHAVIOR OF INTENSITY

4.1. Highly Penetrable Bottom Boundary

Statistical modeling of intensity (4) was performed for two types of bottom boundaries of a shallow-water waveguide: a highly penetrable interface, $c_1 = c = 1460$ m/s, which is often found on the shelf of Arctic seas with increased gas saturation in bottom sediments [33], and boundaries with significant reflectivity, $c = 1460$ m/s, $c_1 = 1600$ m/s. Let us first consider a highly penetrable bottom boundary. In this case, as was shown for volume fluctuations of the sound speed in the water layer in [21, 24], as well as for fluctuations of the impedance function $g_m(r)$ in [25], the maximum statistical effect is observed during propagation of a sound signal. Based on the information from [15], as well as for purposes of comparison with the conclusions of [23], the characteristic scale of variation in $H(r)$ was selected as $L_h = 20$ m, which corresponds to the inhomogeneities of the interface on a fairly small scale. In order of magnitude, they are comparable to the wavelength of the sound signal, but still L_h is more than three times higher than λ. Taking into account also the existing anisotropy along the horizontal coordinate, $L_h \gg \sigma_h$ (a certain degree of smoothness, although insignificant, is present in the statistical problem), which leads to fairly rapid convergence of series (2) of the cross-sectional method. When calculating individual implementations, six modes were taken into account, determining the sound field at distances $r > 300$ m. In mode type, as in all previous studies by the authors [19–25, 29, 30], reference was made to the Pekeris cut on the complex plane of wave numbers $\kappa(r)$, so the square root in $g_m(r)$ is understood in the sense of the main meaning [33, 34]. In the considered case of a highly penetrable bottom boundary, the modes of the discrete spectrum are leaky, their eigenvalues κ_m are complex and, except for the first $\kappa_1(r)$, have a significant imaginary part. The first mode has the largest characteristic attenuation scale $L_{\kappa 1} \sim (\mathrm{Im}\,\kappa_1)^{-1} \approx 2$ km; the scale of the sixth mode, $L_{\kappa 6} \approx 151$ m, differs by more than an order of magnitude. However, in any case, the inequality $L_{h.} \ll L_\kappa$ is satisfied, allowing intense intermode coupling due to the roughness of the boundary. Distances near the source $r < 100$–300 m, where the contribution from the continuous spectrum of horizontal wave numbers κ [34] can be significant, are of no interest from the viewpoint of statistical effects and are therefore not analyzed in this article. Strictly speaking, the continuous spectrum of values κ (in our case these are values on the Pekeris cut, and in the case of discretization of the cut, the corresponding modes are logically called cut modes [30]) is involved in solving problem (2)–(3) through the mode coupling matrices $V(r)$ and $V^T(r)$. Due to mode coupling, when a signal propagates in a waveguide with a penetrable boundary, some of the energy will be transferred from the leaky modes to the cut modes. However, as shown in [29, 30] for a wedge-shaped waveguide shelf with large boundary slope angles (from 6° to 27°), taking into account such modes of the cut in addition to the usual waveguide modes is almost completely unnoticeable along the main propagation distance. The cut modes (continuous spectrum) are significant only at very low frequencies <100 Hz and in local areas where the propagating modes are cut off (the cut modes in these places provide smooth changes in the signal field). In the considered problem there are no significant differences in the depth of the waveguide, $\delta h(r) \ll H(r)$, and mode cutoff does not occur during signal propagation. Therefore, without limiting the generality of the results of the statistical analysis, the contribution of the continuous spectrum for the given model can be neglected. Specially performed calculations taking into account the cut modes showed that the error of neglecting the continuous spectrum for the studied models and propagation distances does not exceed 0.1 dB.

Figures 2–4 show the results of numerical modeling of the behavior of the average signal intensity in the water layer of a randomly inhomogeneous waveguide, which are compared with the intensity during signal propagation in a deterministic waveguide with a unperturbed interface H. From the curves presented in Figs. 2, 3, it is evident that the bathymetry fluctuations $\delta h(r)$, which, as is known from the literature, scatter the signal, increasing propagation losses. However, in [23] it was shown that this effect in the low-frequency region is very small for large- and medium-scale inhomogeneities, $L_h = 1$ km and $L_h = 100$ m, so it can be neglected against the background of the presence of volumetric inhomogeneities in the sound speed in the medium. In the situation of smaller-scale fluctuations of the interface, as follows from Figs. 2 and 3, the decrease in signal intensity in the waveguide at a distance of $r = 20$ km is enhanced to ≈ 9 dB compared to the deterministic case of a horizontal boundary. In this case, the average intensity loss during signal propagation amounts to several decibels already at a distance $r \approx 5$ km. To confirm the result obtained in Fig. 4 for one of the random sampling, the OWP curves obtained by our method (3) with the curves calculated by the well-known RAM program, which implements the wide-angle parabolic equation (WAPE) method [35]. Clearly, almost along the entire propagation path 0.5 km < r < 20 km, the difference between compared curves *1* and *2* and *3* and *4*, taken for different horizons of orientation of the source and receiver, does not exceed 1.5 dB. In practical terms, this means good agreement between the results obtained by different methods and indicates the adequate nature of the decline in the intensity curves in Figs. 2 and 3.

The increase in signal intensity decay established above is explained by the strong mode coupling and intense energy exchange occurring between them in the random waveguide considered. As can be seen from Fig. 5, where the intensity of the field of individual coupling modes forming the signal is presented, the sound energy of the least attenuated and most energy-carrying first mode (for the considered source

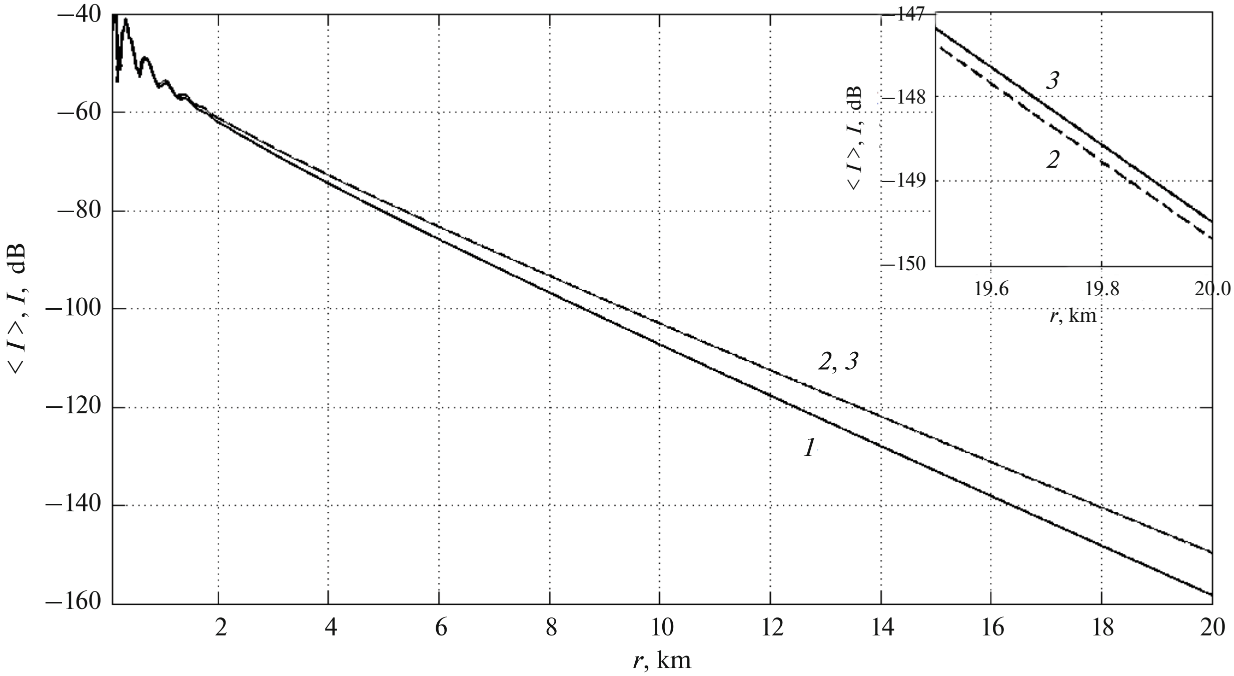

Fig. 2. Decay of average intensity of 250 Hz signal in waveguide with fluctuations of penetrable bottom boundary (bathymetry), $z_0 = z = 24$ m, $L_h = 20$ m. On graph: curve *1*, forward scattering (OWP) approximation (solution (3) for mode amplitudes); dashed curve *2*, adiabatic approximation, $V_{mn} = 0$; curve *3*, horizontal bottom boundary H ($\delta h = 0$). Upper right corner, distance range 19.5–20 km for better visualization of difference between curves *2* and *3* at large distances.

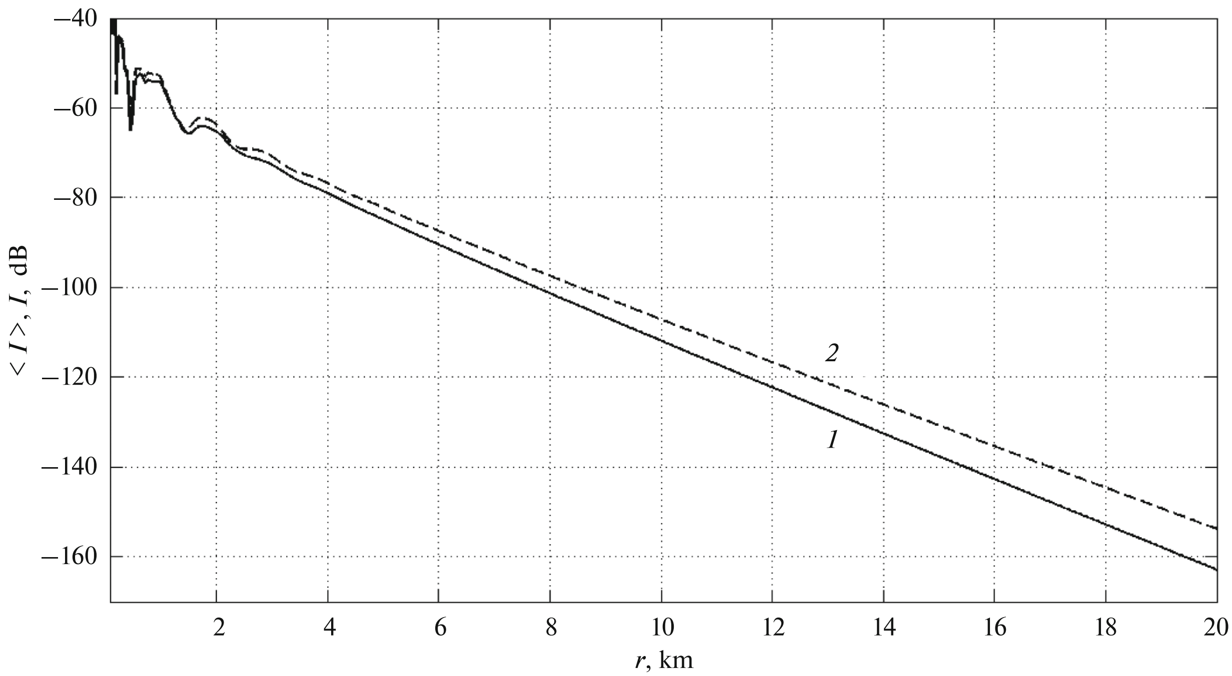

Fig. 3. Curves are similar to Fig. 2, but source and observation horizons are near bottom: $z_0 = 36$ m, $z = 32$ m.

horizon $z_0 = 24$ m first eigenfunction of the waveguide has a maximum) is transferred to modes with higher numbers. However, as has been noted many times before [21–25] and is clear from the comparison of the intensity propagation losses in Figs. 2 and 3, the statistical effect (but not the absolute value of the intensity

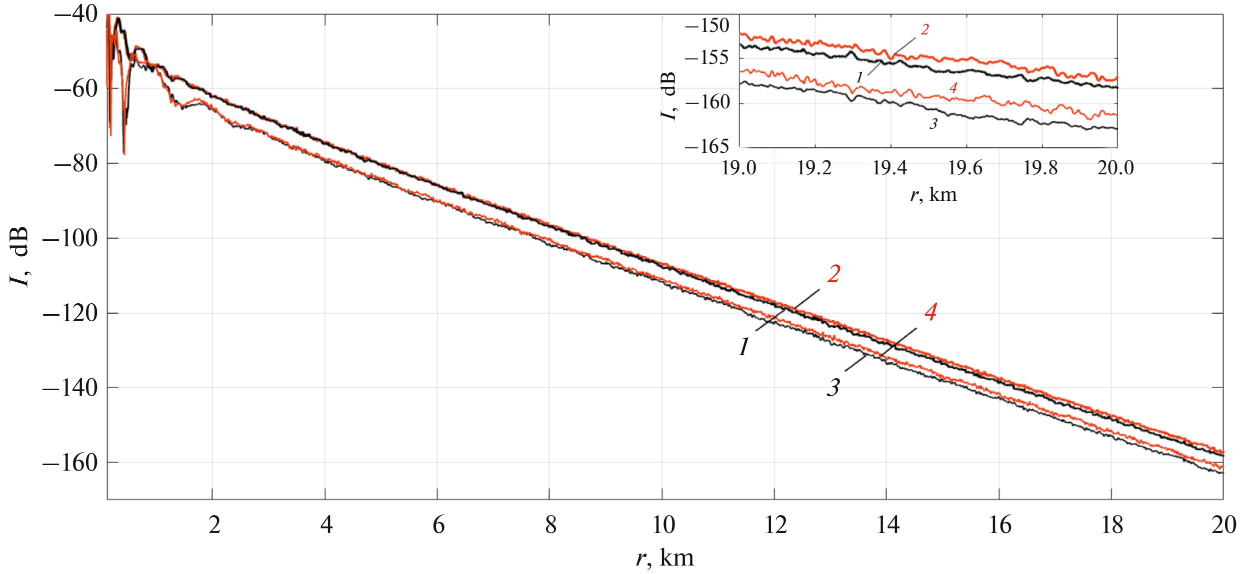

Fig. 4. Comparison of 250 Hz signal intensity curves in waveguide with fluctuations of penetrable bottom boundary for some arbitrary random sampling $\delta h(r)$, $L_h = 20$ m. On graph: curve *1* is OWP approximation (solution of Eq. (3)), curve 2 is calculation by RAM program using WAPE method, $z_0 = z = 24$ m; curve *3*, OWP approximation; curve *4*, calculation by RAM program using WAPE method, $z_0 = 36$ m, $z = 32$ m.

level) depends weakly on the horizon of the source location. A specific feature of the energy redistribution between local modes is their fairly rapid transformation over a segment with a distance of 100 m–2 km. Comparison with the curves of the adiabatic approximation (dashed curves in figures) shows that with distance there is a decrease in the average intensity of the first mode, due to which an increase in the intensity level of all other modes (second–sixth) is observed. Moreover, the intensity levels of higher modes, starting from the second, at $r > 2$ km are found to be concentrated in a fairly narrow range ≈ 8 dB between the third and fourth modes shown in Fig. 5. It is interesting to note that from distances of approximately 2–3 km, all transformed modes in a statistical sense have a similar mode attenuation coefficient, which for mode numbers $m > 1$ becomes significantly smaller than it was for local modes at the beginning of the path, near the source localization (there it corresponds to the adiabatic and deterministic solutions). This is clear from a comparison of the solid and dashed mode intensity curves of the corresponding numbers in Fig. 5. As a result, the difference between the intensity levels of individual modes acquired at the original segment of 0.1 km $< r <$ 3 km (e.g., the difference in level for nearest first and third modes at $r \approx 3$ km is ≈ 21–22 dB), then changes little along the propagation path, and the decay curves of all modes run almost parallel to each other. In this case, the curves of the OWP approximation modes, including all higher modes, are located between the curves of the first and second modes of the adiabatic approximation and the unperturbed waveguide (dashed curves *1* and *2* in Fig. 5). Figure 5 shows that, despite the strong mode coupling in a random waveguide, the overwhelming contribution to the signal field under conditions of a highly penetrable bottom boundary comes from the first mode. At $r > 2$ km the difference between the levels of average signal intensity and the levels for its first mode does not exceed 0.5 dB. It is also important to make a remark regarding the adiabatic approximation. Although this approximation takes into account fluctuations in the mode eigenvalues under the influence of random irregularities of the interface (see Fig. 1b), for the intensity, it virtually coincides with the deterministic solution in a waveguide with a horizontal bottom boundary (Fig. 2 and the inset in the right corner of this figure). Therefore, the adiabatic approximation does not describe the true statistical solution, which was already discussed above in the section on formulation of the problem. It should be emphasized that in each individual sampling, the adiabatic approximation also gives an incorrect solution, which differs even more from the OWP solution than the average statistical one in Figs. 2 and 3. One of the reasons for this is the indicated fact of the overwhelming contribution of the first mode to the signal field. Fluctuations of the boundary, as can be seen in Fig. 1b, cause the greatest perturbations of the eigenvalues not of the first modes, but of modes with higher numbers. However, they quickly decay with distance and do not contribute to the signal propagating in the waveguide. In this case, in the adiabatic approximation, the value of the characteristic scale of fluctuations L_h does not affect the fact that the statistical solution differs weakly from the

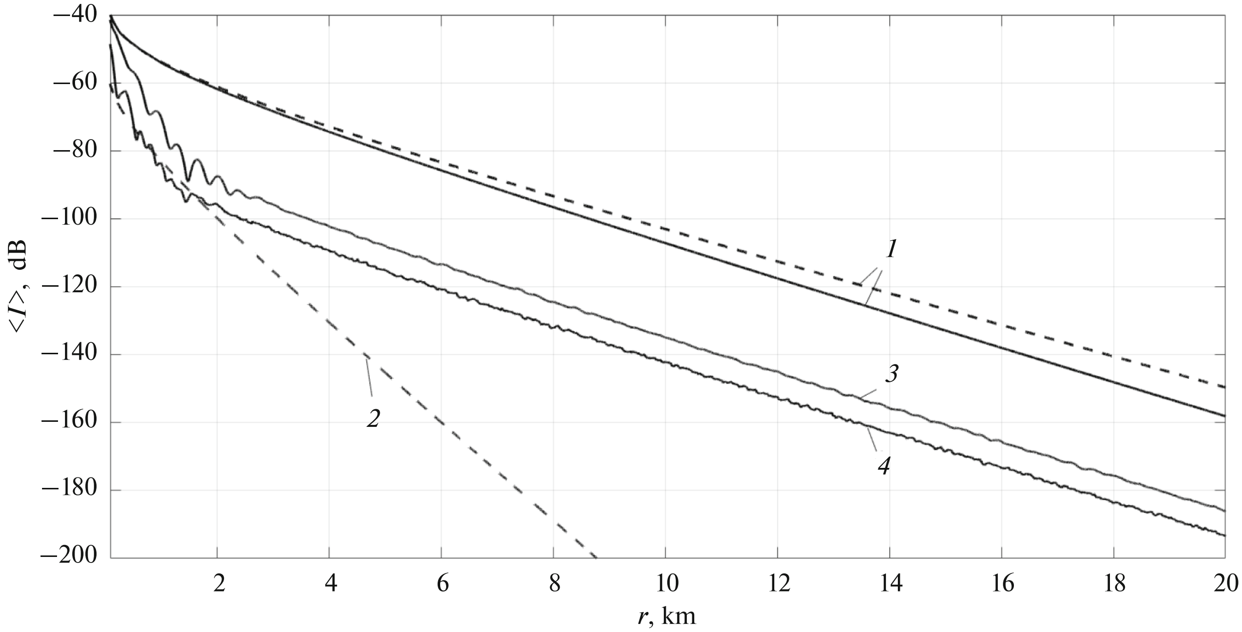

Fig. 5. Average intensity of individual modes of 250 Hz signal in waveguide with fluctuations of bottom boundary, $L_h = 20$ m, $z_0 = z = 24$ m. Solid curves *1*, *3*, *4* are intensities of modes of these numbers in forward scattering (OWP) approximation; dashed curves *1*, *2* are adiabatic approximation ($V_{mn} = 0$).

deterministic one. For "adiabatic" scattering, the same conclusion is valid in the case of inhomogeneities of the boundary of both media, $L_h = 100$ m, and large scales, $L_h = 1$ km [23].

Figures 6 and 7, using the scintillation index S, present additional information on fluctuations in the sound field intensity in the waveguide [31, 36], which confirms the specific behavior of modes in the waveguide under the influence of a statistically rough water–bottom sediment interface. Note the following. Fluctuations in the intensity (scintillations) of the sound field in the waveguide are generally characterized by fairly small values, which are inherent in the fluctuations of the intensity of the first mode along the entire propagation path: $S_1 < 0.25$. The intensity fluctuations are particularly small, $S \ll 1$, for the solution in the adiabatic approximation (Fig. 6, curves *1*).

Except for the distance range $r < 3$ km, where oscillations of the interference structure are present (as in Fig. 5 for individual coupling modes), the scintillation curves on the graphs in Fig. 6 are quite monotonic. The slow growth of the curves with distance is due to the monotonic decrease in the average intensity in the waveguide. Figure 7 shows that for individual modes, the range 0.1 km $< r <$ 2 km of transition to establishment of a stationary regime of fluctuation saturation ends quite quickly. As expected, the higher the mode number, the more pronounced the fluctuations in its intensity are (cf. Fig. 1b). So, for the mode with the number $m = 6$, scintillations exceed level 1, that is, the intensity fluctuations of this mode are strong; their magnitude is comparable to the level of the average intensity itself. However, this does not in any way affect the pattern of average losses during propagation due to the smallness of the absolute intensity level of higher-number modes.

4.2. Reflective Bottom Boundary

Let us now conduct a comparative analysis of the results obtained above for a highly penetrable randomly inhomogeneous bottom boundary with the results for the reflecting boundary of the waveguide: $n \approx 0.91(1 + 0.02i)$, $c_1 = 1600$ m/s. For a boundary with such an impedance, six propagating coupling modes are formed in the water layer of the waveguide; in addition, three leaky modes were taken into account in numerical modeling. Since the number of weakly damped modes is now increased, the intensity pattern in the waveguide is characterized by an oscillatory structure due to intermode interference, which is expressed not only in the first few hundred meters of the path, but also at long distances. This is especially true when the source and observation points are located near the bottom. In order to analyze statistical effects without complicating the graph material with details of the interference structure, let us consider, where it makes sense, spatially smoothed dependences of the intensity and its scintillations, i.e., expression (4) for the incoherent sum of modes ($m = l$). Figure 8, similar to Fig. 1b, shows fluctuations in the eigenval-

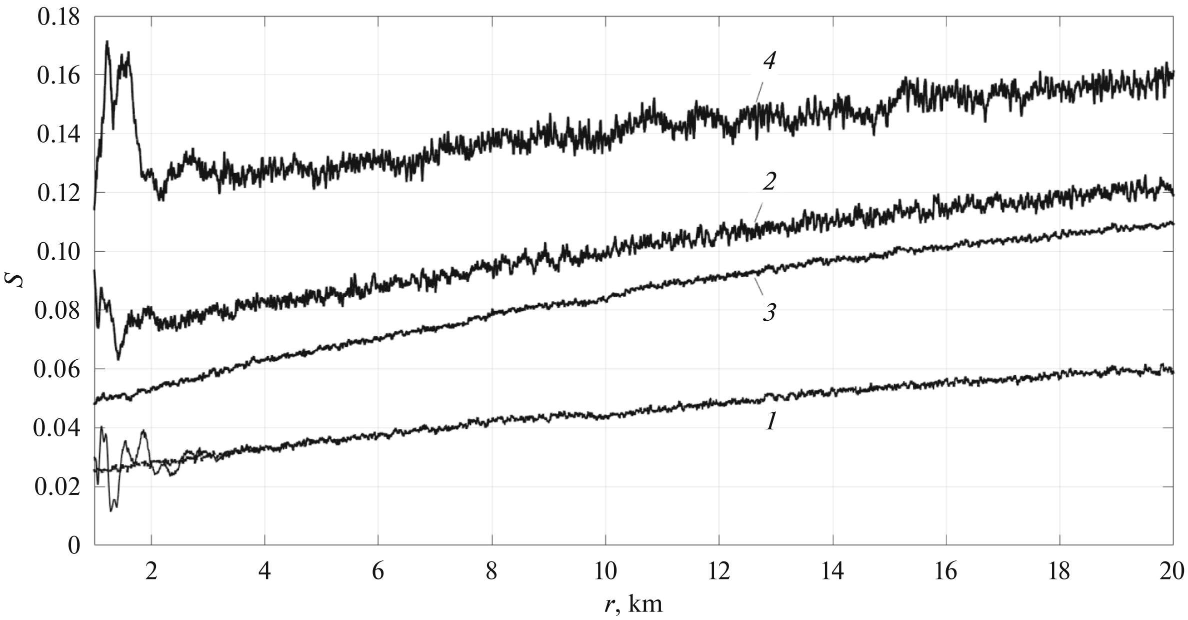

Fig. 6. Development of scintillation index of sound field intensity and individual modes in waveguide with statistically rough highly penetrable boundary, $L_h = 20$ m, $z_0 = z = 24$ m. Curves correspond to curves in Fig. 5: (*1*) fluctuations in intensities of total field and field of first mode (dash is visible on graph at beginning of path) in adiabatic approximation; (*2*) forward scattering, fluctuations in intensity of total field; (*3*) similar to curve *2*, but for first mode; (*4*) fluctuations of total field intensity for $z_0 = 36$ m, $z = 32$ m.

ues $\kappa_m(r)$ along the propagation path of the waveguide in one arbitrary sampling. Clearly, the amplitude of fluctuations in the eigenvalues of higher modes increases; the variance can reach 5–10%, so that the ranges of variation in $\kappa_m(r)$ begin to intersect (e.g., for $\kappa_8(r)$ and $\kappa_9(r)$). Since $V_{mn} \sim (\kappa_m - \kappa_n)^{-1}$, for such distances, the coupling of neighboring higher modes will obviously be enhanced. However, this does not manifest itself in the behavior of the total field intensity due to its very low level for higher modes.

The graphs in Fig. 9 indicate that in the case of a reflective rough bottom boundary, compared to a highly penetrable boundary (cf. curves in Fig. 2), attenuation of the average intensity is significantly reduced (by ≈8 dB at a distance of 20 km), so that the difference between the OWP curves and curves of the adiabatic approximation and a horizontal bottom is no greater than 1 dB. In this case, local modes with numbers $m > 1$ propagate better, their mode attenuation coefficient due to interaction with the bottom is much smaller. Therefore, in the case of a reflective boundary, the portion of energy that is redistributed in the waveguide between the first four weakly attenuating modes and the high-numbered modes subject to more significant attenuation turns out to be significantly smaller compared to the situation for a highly penetrable boundary. These features are reflected in Fig. 10 (cf. Fig. 5). In the case of a reflecting boundary at the beginning of the propagation path, local modes of higher numbers, "pulling" energy from the first modes, have a lower mode attenuation coefficient; i.e. their energy is transferred more weakly from the water layer of the waveguide to the sedimentary layer at the stage of formation of the modes of the stochastic waveguide 0.1 km $< r <$ 12 km. At $r >$ 12 km, all waveguide modes acquire a similar mode attenuation coefficient, which is significantly smaller in magnitude for the reflecting boundary than for the penetrable boundary. The difference between the intensity levels of individual modes acquired over a segment 0.1 km $< r <$ 12 km (e.g., the difference in the levels of the curves for the nearest first and third modes at $r \approx$ 12 km is ≈ 30 dB), then changes little along the propagation path.

Declining curves of modes with numbers $m > 1$ run almost parallel to each other in a narrow intensity range ≤ 10 dB, and the curves of all nine modes of the OWP approximation are located between the curves of the first and fourth modes of the adiabatic approximation (dashed curves *1, 4* in Fig. 10). In Fig. 11, a comparison of the laws of intensity decay, averaged over the spatial scale of interference, for different horizons shows patterns similar to the curves in Figs. 2 and 3 for a highly penetrable bottom interface of a random waveguide; however, the difference in the levels of the OWP and adiabatic curves is significantly smaller, within ≈ 1 dB. The adiabatic approximation, shown by the dashed curves, in this case also corresponds almost completely to a waveguide with a horizontal flat bottom, i.e., in the absence of disturbances of the bottom boundary.

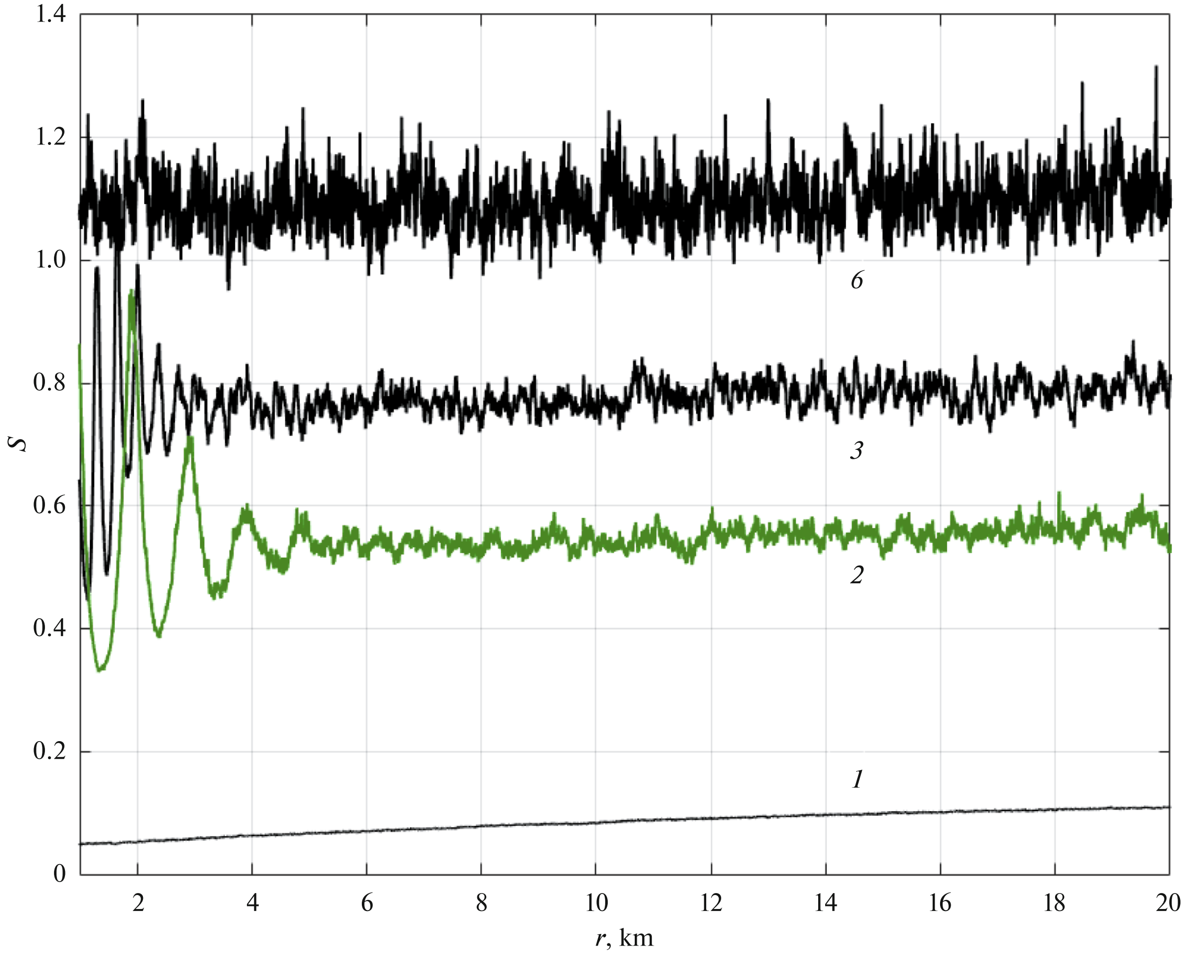

Fig. 7. Development of scintillation index of intensity of individual modes in waveguide with statistically rough highly penetrable boundary, $L_h = 20$ m, $z_0 = z = 24$ m. Curves on graph are scintillations of modes with indicated numbers *1*, *2*, *3*, *6*.

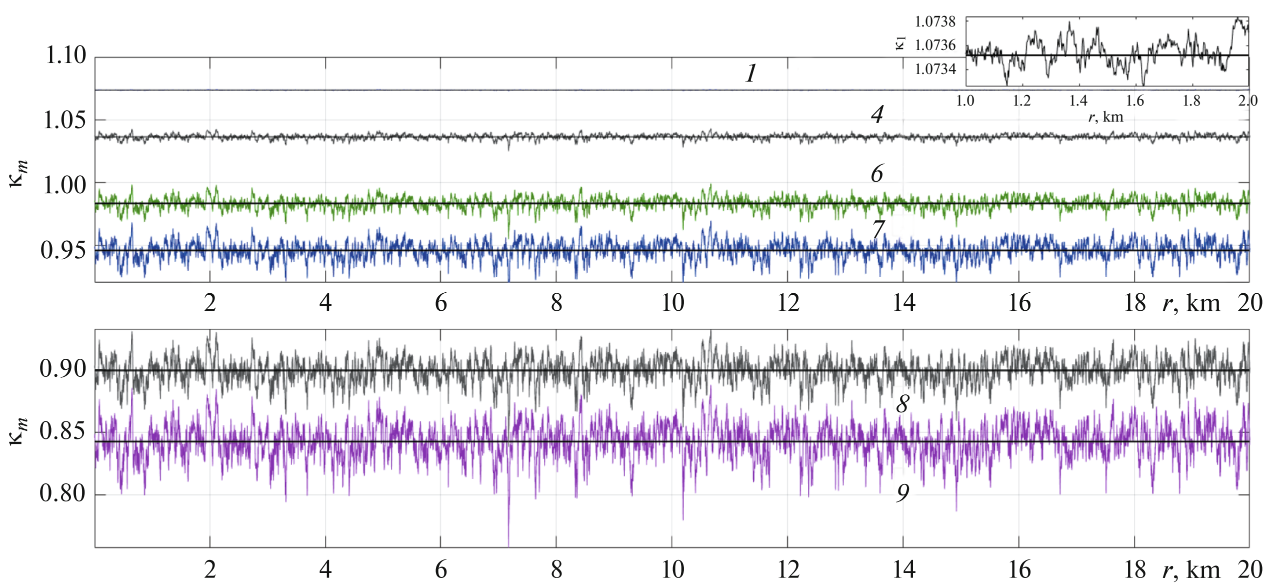

Fig. 8. Illustration of model of stochastic waveguide with a reflecting bottom boundary. Arbitrary random sampling of real part of eigenvalues $\kappa_m(r)$ of numbers m = 1, 4, 6, 7–9. L_h = 20 m. Horizontal lines on graphs are eigenvalues for unperturbed waveguide. Insert in upper right corner, sampling segment1 km < r < 2 km of first eigenvalue $\kappa_1(r)$.

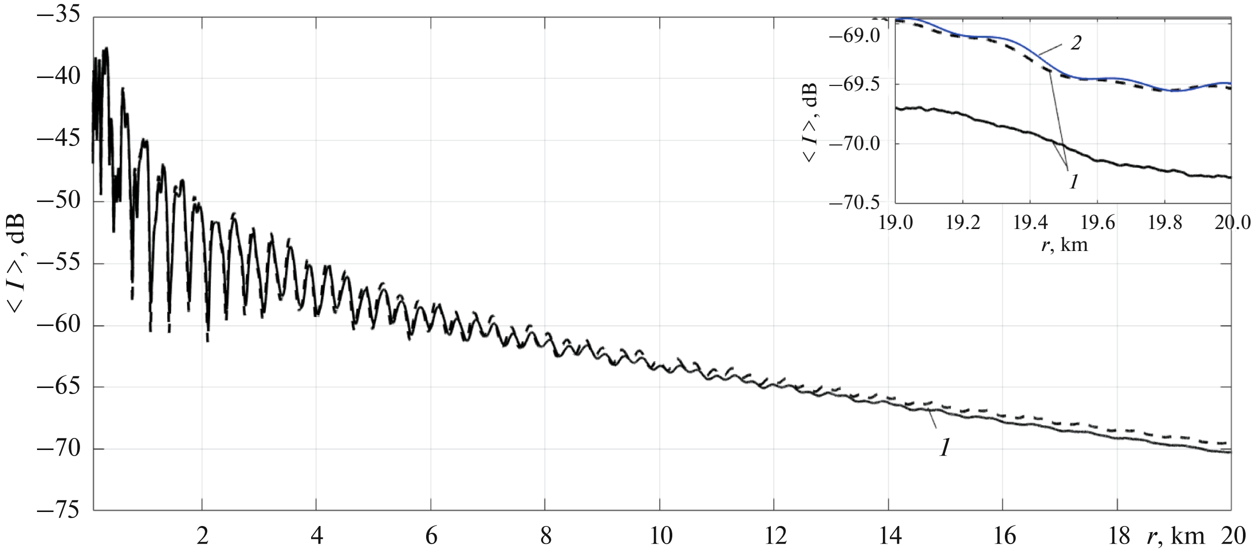

Fig. 9. Decay of average intensity of 250 Hz signal in random waveguide with fluctuations of reflecting bottom boundary, $z_0 = z = 24$ m, $L_h = 20$ m. On graph: curves *1*, forward scattering approximation (3); dashed curve, adiabatic approximation ($V_{mn} = 0$); curve *2*, horizontal bottom boundary H ($\delta h = 0$). Upper right corner, distance range 19–20 km for detailing curve structure at end of path.

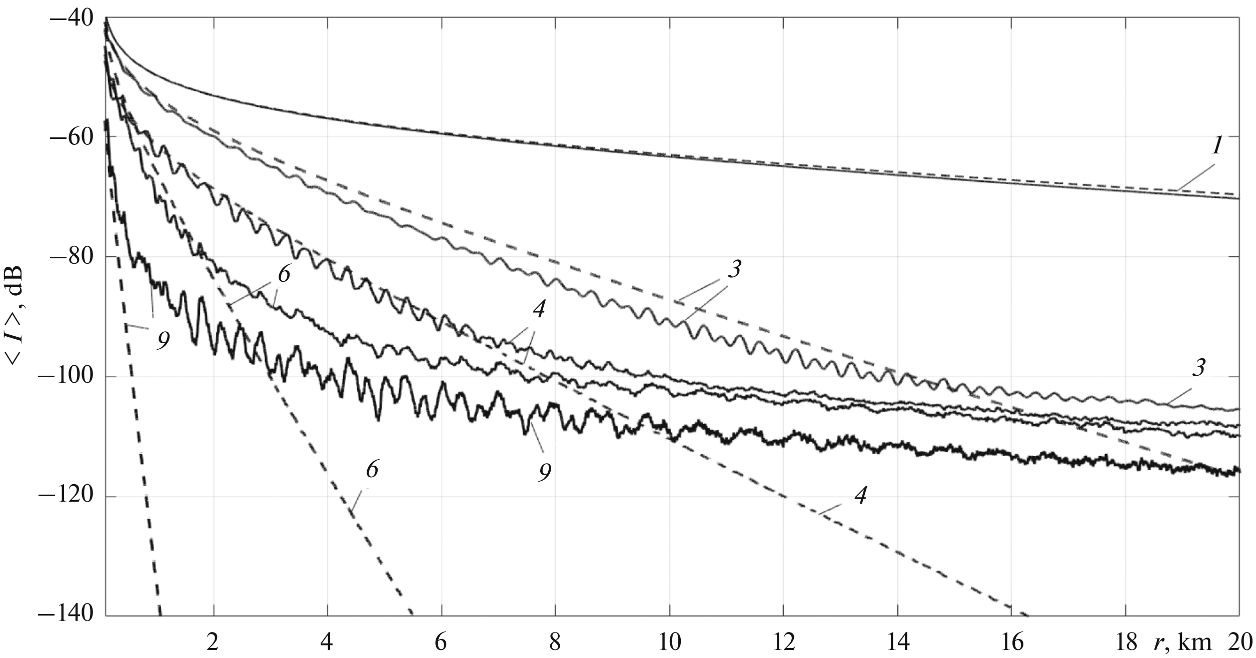

Fig. 10. Average intensity of individual modes of 250 Hz signal in waveguide with fluctuations of reflecting bottom boundary, $L_h = 20$ m, $z_0 = z = 24$ m. Solid curves *1*, *3*, *4*, *6*, *9* are intensities of modes of these numbers in forward scattering (OWP) approximation; dashed curves, adiabatic approximation.

The scintillation curves in Fig. 12 for the sums of incoherent mode in (4) obviously indicate the absence of strong fluctuations in signal intensity, but for the localization of the source and receiver near the rough bottom boundary, where the contribution of higher-numbered modes is more significant, these intensity fluctuations are somewhat larger than for the middle part of the waveguide. Compared to the case of a highly penetrable bottom boundary, the signal scintillations in Fig. 12 are characterized by approximately the same levels, and in general the curves are similar to the curves in Fig. 6. For individual modes, the scintillation graphs do not provide additional information compared to Fig. 7 and are therefore not presented here.

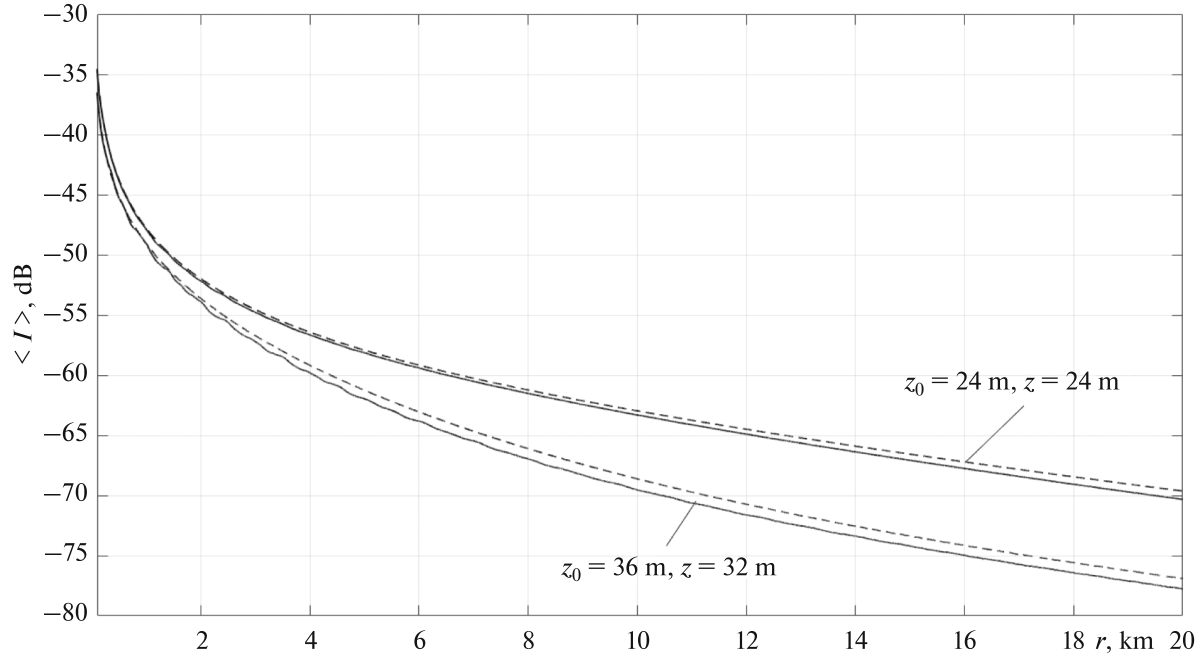

Fig. 11. Average intensity of 250 Hz signal in random waveguide with fluctuations of reflecting bottom boundary for different source and receiver locations, $L_h = 20$ m. Solid curves, forward scattering approximation (3) for $z_0 = 36$ m, $z = 32$ m, and $z = z_0 =$ 24 m; dashed curves, adiabatic approximation for indicated horizons.

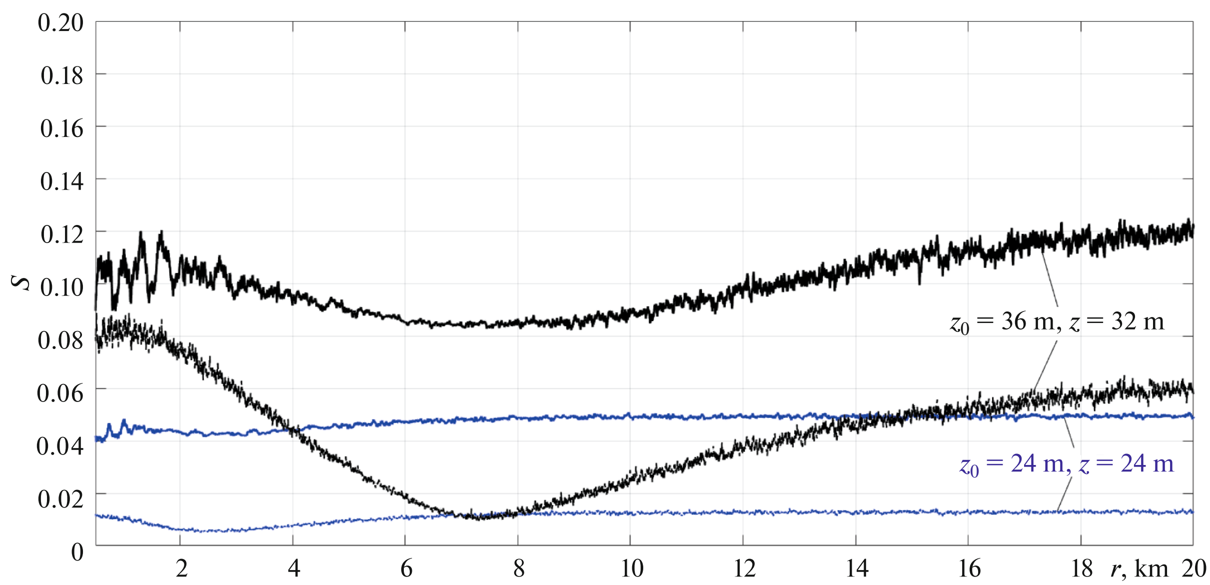

Fig. 12. Development of scintillation index of sound field intensity in waveguide with statistically rough reflective boundary, $L_h = 20$ m. Solid curves, forward scattering for horizons $z_0 = z = 24$ m and $z_0 = 36$ m, $z = 32$ m. Dashed curves (lower), adiabatic approximation for same horizons.

5. CONCLUSIONS

In this article, the behavior of average intensity values and their scintillations during the propagation of a low-frequency sound signal in a stochastic waveguide with a randomly rough bottom boundary is investigated using statistical modeling. The situation of fairly small-scale boundary irregularities with not too small fluctuation amplitude is considered. In addition, two types of rough boundaries are analyzed: a highly penetrable bottom boundary and a boundary with significant reflectivity. The waveguide itself, from the viewpoint of stratification of the parameters, was assumed to be homogeneous, both in the water layer and in the liquid bottom sediments, which made it possible to abstract from disturbances of the sound signal by volumetric inhomogeneities in the sound speed and to study in its pure form the features of the influence of random fluctuations of the bottom boundary. In practical terms, a waveguide of this type can serve as a good model of shallow-water sound propagation in areas of some seas of the Arctic shelf. It is in these latitudinal regions that, from both a theoretical and a field observational viewpoint, internal waves are almost absent (probably with the exception of the relatively deep Barents Sea in the summer season), which in most other regions of the World Ocean are the main random disturbance leading to volumetric fluctuations in the sound speed and stochastic behavior of acoustic signals. The statistical modeling performed showed the following.

1. Small-scale disturbances of the bottom boundary can lead to noticeable changes in the law of decay of the average signal intensity in shallow water. The attenuation of intensity at distances of 10–20 km, typical for shallow-water sound propagation in Arctic shelf zones with gas-saturated sediments, under the influence of random disturbances of the bottom boundary can reach 5–10 dB.

2. This result differs from the previously obtained conclusion for medium-scale and large-scale irregularities of the penetrable boundary [23], which, as it turned out, have practically no effect on the propagation of the signal in the waveguide, therefore, against the background of other irregularities, large-scale fluctuations of the boundary can be neglected.

3. The obtained result of the influence of small-scale fluctuations of the water-bottom sediment interface, leading to energy losses of the signal with distance, is directly opposite to the influence of volumetric random inhomogeneities of the sound speed on the signal. The latter are present in the thickness of bottom sediments of the shallow shelf of the Arctic seas, or in the water layer of seas of lower latitudes, which have stratification and disturbances in the form of internal waves. Large-scale volumetric inhomogeneities of the sound speed lead not to an increase, but to a weakening of the decrease in the average intensity in the waveguide [20–22, 24].

4. The specific behavior of the intensity of individual modes in an arctic-type waveguide with small-scale irregularities of the bottom boundary is manifested in the strong coupling of local modes. As a result of the transformation, the first mode in the waveguide, as a rule, the most energy-carrying and weakly damped, quite quickly (at a distance of 2–3 km) transfers a significant part of its energy to higher modes. For this reason, in comparison with the region of distances adjacent to the source, an increase in the attenuation of the first mode is observed, while the modes of higher numbers, conversely, acquire a significantly smaller (original) mode attenuation coefficient, which actually differs little from the coefficient of the first mode. However, in a waveguide with a highly penetrable bottom boundary, the total signal intensity along the entire propagation path is determined mainly by the intensity of the first mode.

5. Changing the impedance properties of the bottom boundary from strong sound transmission to significant reflection does not fundamentally change the effect of small-scale disturbances of the boundary. The average intensity also attenuates in the waveguide due to the energy losses of the first (first, second, third, and fourth) modes, but attenuates much more slowly, since at the beginning of the propagation path, local modes of higher numbers, “pulling” energy from the first modes, have a lower mode attenuation coefficient, i.e. they carry away energy from the water layer of the waveguide into the sediments less strongly.

6. The scintillation index in the problem considered demonstrates features that confirm the conclusions regarding the behavior of the average signal intensity. The pattern of average intensity fluctuations shows the presence of two distance regions in the waveguide. The original segment corresponds to distances up to 2–10 km (depending on the type of boundary), at which intensive redistribution of energy between local modes occurs and stochastic waveguide modes are formed. The second region is characterized by monotonic behavior of scintillations associated with the achievement of a quasi-stationary fluctuation saturation regime. However, for both types of boundaries, both penetrable and reflecting, the scintillation index indicates the absence of strong intensity fluctuations during signal propagation in a waveguide with a randomly rough bottom boundary. This conclusion differs from the behavior of intensity fluctuations in a waveguide with random volumetric inhomogeneities of the sound speed.

7. The adiabatic approximation, which does not take into account mode coupling, for a waveguide with small-scale fluctuations of the bottom boundary leads to incorrect results, both in statistical terms and in individual realizations of the signal intensity. This is primarily evident for the highly penetrable bottom boundary, as well as for individual modes that form the field. The adiabatic solution differs little from the solution for a waveguide with an unperturbed horizontal boundary. This is due to the boundary condition of the plane-layered comparison waveguide, which is used in calculations using the adiabatic approximation. Therefore, the results of the adiabatics differ greatly from the conclusions for randomly inhomogeneous waveguides with volume fluctuations of the sound speed (but horizontal boundaries), where the adiabatic solution for the average intensity is often

close to OWP solution (3), which takes into account mode coupling in a perturbed waveguide.

APPENDIX A

BRIEF DERIVATION OF EMBEDDING EQUATIONS FOR THE AMPLITUDES OF MONOCHROMATIC SIGNAL MODES IN THE CASE OF A TWO-DIMENSIONALLY INHOMOGENEOUS MEDIUM IN AN AXIALLY SYMMETRIC FORMULATION OF THE PROBLEM.

Instead of the second-order equation for sound pressure (1), for further derivation it is convenient to consider the linear first-order acoustics equations for sound pressure fields p and the particle velocity component—w, vertical; v, horizontal—with the corresponding conditions, formulated in Section 2, of continuity of these functions, boundary conditions along the vertical coordinate z on the sea surface and bottom, and the radiation conditions

$$\frac{\partial p(r,z)}{\partial z} = i\omega\rho(r,z)w(r,z),$$
$$\frac{\partial p(r,z)}{\partial r} = i\omega\rho(r,z)v(r,z),$$
$$\rho(r,z)\left[\frac{\partial w(r,z)}{\partial z} + \left(\frac{\partial}{\partial r} + \frac{1}{r}\right)v(r,z)\right] - \frac{i\omega}{c^2(r,z)}p(r,z) = \frac{i\delta(r)\delta(z-z_0)}{\omega r}.$$

According to the cross-sectional method, we seek a solution in the form of convergent expansions in local modes (comparison waveguide modes):

$$p(r,z) = \sum_{m=1}^{M} G_m(r)\varphi_m(r,z);$$
$$w(r,z) = [i\rho(r,z)\omega]^{-1}\sum_{m=1}^{M} G_m(r)\,\partial\varphi_m(r,z)/\partial z; \quad \text{(A1)}$$
$$v(r,z) = [i\rho(r,z)\omega]^{-1}\sum_{m=1}^{M} F_m(r)\varphi_m(r,z).$$

Substituting expansions (A1) into the equations taking into account the property of orthonormality of modes leads to equations for the mode amplitudes $G_m(r)$ and $F_m(r)$, $m = 1\ldots M$:

$$\frac{\partial G_m(r)}{\partial r} = F_m(r) - \sum_{l=1}^{M} V_{ml}(r)G_l(r),$$
$$\frac{\partial F_m(r)}{\partial r} = -\frac{F_m(r)}{r} - \kappa_m^2 G_m(r) + \sum_{l=1}^{M} V_{lm}(r)F_l(r) - \frac{\delta(r)}{2\pi r}, \quad \text{(A2)}$$

$$\{V_{lm}(r)\} = V^T(r) = -V(r) - \int_0^\infty \varphi_m(r,z)\varphi_l(r,z)\frac{\partial}{\partial r}\left(\frac{1}{\rho(r,z)}\right)dz.$$

Let us now formulate the boundary value problem for Eqs. (A2) in the horizontal plane as follows. We assume that the medium, which is inhomogeneous in the horizontal plane, is located within the boundaries $r \in (L, L_0)$ and is at some arbitrary distance from the source, which is placed at the origin of the cylindrical system. It is convenient to consider the wave zone of the source, $\kappa_m L \gg 1$, since the statistical effects of interest to us appear at significant distances from the source. In this case, in the second equation of the system, the term $F_m(r)/r$ should be neglected due to its smallness, and when formulating the boundary conditions, we should switch from cylindrical functions to exponentials. From functions $G_m(r)$, $F_m(r)$ it is expedient to single out the factor of cylindrical divergence $D(r) = i[8\pi i r]^{-1/2}$, which arises in the asymptotics of cylindrical functions and does not affect the derivation of subsequent equations. In the ranges $0 < r \le L$, $r \ge L_0$ inhomogeneities in r are absent; i.e., the medium is plane-layered with mode number values $\kappa_m = \kappa_m^0$ and $\kappa_m = \kappa_m^1$. The type of solution in these regions is known, since it is described by homogeneous Eqs. (A2) with constant coefficients without mode coupling:

$$\frac{\partial G_m(r)}{\partial r} = F_m(r), \quad \frac{\partial F_m(r)}{\partial r} = -\kappa_m^2 G_m(r),$$
$$\kappa_m r \gg 1, \quad \kappa_m = \{\kappa_m^0, \kappa_m^1\}.$$

$$\begin{gathered} G_m(r) = j_m(0,z_0)(k_m^0)^{-1/2}\{\exp[ik_m^0 r] + R_m(L)\exp[-ik_m^0(r-L)]\}, \quad 0 < r \le L; \\ G_m(r) = T_m(L_0)(k_m^1)^{-1/2} \times \exp[ik_m^1(r-L_0)], \quad r \ge L_0, \end{gathered} \quad \text{(A3)}$$

where $R_m(L)$ is the mode reflection coefficient in section $r = L$, and $T_m(L_0)$ is the mode transmission coefficient in section $r = L_0$. Thus, the original conditions to formulate the boundary value problem for mode amplitudes for $r \in (L, L_0)$ are the following

$$\begin{gathered} \frac{\partial G_m(r)}{\partial r} = F_m(r) - \sum_l V_{ml}(r)G_l(r), \\ \frac{\partial F_m(r)}{\partial r} = -\kappa_m^2(r)G_m(r) + \sum_l V_{lm}(r)F_l(r), \end{gathered} \quad \text{(A4)}$$

and expressions (A3) in layered regions of the medium $0 < r < L$, $r > L_0$. Based on the continuity of functions $G_m(r)$, $F_m(r)$, the boundary conditions for Eqs. (A4) can be formulated as follows:

$$i\kappa_m(L)G_m(L) + F_m(L) = a_m(L), \quad \text{(A5)}$$

$$i\kappa_m(L_0)G_m(L_0) - F_m(L_0) = 0. \tag{A6}$$

Here $a_m(L) = 2i\varphi_m(0,z_0)\kappa_m^{1/2}(L)\exp[i\kappa_m(L)L]$ describes the amplitude of the source induced in the section $r = L$ of the incident mth mode. The second condition (A6) corresponds to the free passage of the mth mode from an inhomogeneous to a layered medium for $r > L_0$. Boundaries of the irregular part of the waveguide (L, L_0) are assumed to be consistent with the layered medium, i.e., $\kappa_m^0 = \kappa_m(L)$, $\kappa_m^1 = \kappa_m(L_0)$ (the jumps in the parameters of the medium are absent or small enough for rapid convergence of expansions (A1)).

To reformulate boundary value problem (A4)–(A6) for mode amplitudes, note that the solution to this problem depends on the position of the boundary L of the region of inhomogeneities to which modes arrive from the source; i.e., the functions $G_m(r)$, $F_m(r)$ depend on L, albeit implicitly. Therefore, acting in a standard manner [37, 38], we consider the parametric dependence of the functions G_m and F_m on the position of the boundary L: $G_m(r) \equiv G_m(r; L)$, $F_m(r) \equiv F_m(r; L)$. Let us emphasize that these are the same functions, only with a separate dependence on the position of the boundary to which the modes arrive from the source. Differentiating with respect to the parameter L Eqs. (A4) and boundary conditions (A5), (A6), comparing them with the original boundary value problem (A4)–(A6) it is easy to see that the structure of the Eqs. (due to their linearity) will not change, as a result for each of the functions $G_m(r; L)$ and $F_m(r; L)$ it is possible to obtain a system of closed equations for the parameter L with the original conditions. Since in this study the embedding equations are needed to carry out calculations, then from the viewpoint of the computational procedure, it makes sense to simplify the boundary value problem (A4)–(A6) by removing unnecessary parameters. To do this, we select a column vector of the amplitudes of the modes $\mathbf{b}(L)$ incident on an irregular medium, with elements $b_m(L) = \varphi_m(0, z_0)\kappa_m^{-1/2}(L)\exp[i\kappa_m(L)L]$, $m = 1...M$, and we consider the solution to the problem of mode transformation in an irregular medium, but with modes with the unit amplitude incident on it [37], based on matrix notation of the following form:

$$\mathbf{G}(r) = G(r;L)\mathbf{b}(L), \quad \mathbf{F}(r) = F(r;L)\mathbf{b}(L),$$

where $\mathbf{G}(r) \equiv \mathbf{G}(r;L)$, $\mathbf{F}(r) \equiv \mathbf{F}(r;L)$ are the column vectors of the mode amplitudes of boundary value problem (A4)–(A6), and $G(r; L)$ and $F(r; L)$ are square matrices of dimension $M \times M$, satisfying the boundary value problem

$$\begin{aligned} \frac{\partial G(r;L)}{\partial r} &= F(r;L) - V(r)G(r;L), \\ \frac{\partial F(r;L)}{\partial r} &= -\kappa^2(r)G(r;L) + V^T(r)F(r;L), \end{aligned} \tag{A7}$$

$$i\kappa(L)G(L;L) + (L;L) = 2ik(L), \tag{A8}$$

$$i\kappa(L_0)G(L_0;L) - F(L_0;L) = 0. \tag{A9}$$

In (A7)–(A9) $\kappa(L)$ is the diagonal matrix of eigenvalues $\kappa_m(L)$, and we immediately included *parameter L* in the number of arguments of functions G and F. After differentiating (A7)–(A9) in terms of L, we obtain the following boundary value problem:

$$\begin{aligned} \frac{\partial}{\partial r}\frac{\partial G(r;L)}{\partial L} &= \frac{\partial F(r;L)}{\partial L} - V(r)\frac{\partial G(r;L)}{\partial L}, \\ \frac{\partial}{\partial r}\frac{\partial F(r;L)}{\partial L} &= -\kappa^2(r)\frac{\partial G(r;L)}{\partial L} + V^T(r)\frac{\partial F(r;L)}{\partial L}, \end{aligned} \tag{A10}$$

$$\begin{aligned} &i\frac{d}{dL}\kappa(L)[G(L;L)] + i\kappa(L)\frac{d}{dL}G(L;L) \\ &\quad + \frac{d}{dL}F(L;L) = 2i\frac{d}{dL}\kappa(L), \end{aligned} \tag{A11}$$

$$i\kappa(L_0)\frac{\partial}{\partial L}G(L_0;L) - \frac{\partial}{\partial L}F(L_0;L) = 0. \tag{A12}$$

Revealing the derivatives in (A11),

$$\frac{dG(L;L)}{dL} = \left.\frac{\partial G(r;L)}{\partial r}\right|_{r=L} + \left.\frac{\partial G(r;L)}{\partial L}\right|_{r=L}$$

and $$\frac{dF(L;L)}{dL} = \left.\frac{\partial F(r;L)}{\partial r}\right|_{r=L} + \left.\frac{\partial F(r;L)}{\partial L}\right|_{r=L},$$

based on (A7), (A8), for brevity denoting the derivative $\kappa'(L) = \dfrac{d}{dL}\kappa(L)$, we obtain

$$\begin{aligned} \frac{\partial}{\partial r}\frac{\partial G(r;L)}{\partial L} &= \frac{\partial F(r;L)}{\partial L} - V(r)\frac{\partial G(r;L)}{\partial L}, \\ \frac{\partial}{\partial r}\frac{\partial F(r;L)}{\partial L} &= -\kappa^2(r)\frac{\partial G(r;L)}{\partial L} + V^T(r)\frac{\partial F(r;L)}{\partial L}, \end{aligned} \tag{A13}$$

$$\begin{aligned} &i\kappa(L)\frac{\partial}{\partial L}G(r;L)\Big|_{r=L} + \frac{\partial}{\partial L}F(r;L)\Big|_{r=L} \\ &= -i\kappa(L)F(L;L) + i\kappa(L)V(L)G(L;L) \\ &\quad + \kappa^2(L)G(L;L) - V^T(L)F(L;L) \\ &\quad - i\kappa'(L)G(L;L) + 2i\kappa'(L) \\ &= 2i\kappa(L)[\kappa^{-1}(L)\kappa'(L) - i\kappa(L) \\ &\quad - \kappa^{-1}(L)V^T(L)\kappa(L)] - i\kappa(L)[\kappa^{-1}(L)\kappa'(L) \\ &\quad - V(L) - \kappa^{-1}(L)V^T(L)\kappa(L)]G(L;L), \end{aligned} \tag{A14}$$

$$i\kappa(L_0)\frac{\partial}{\partial L}G(L_0;L) - \frac{\partial}{\partial L}F(L_0;L) = 0. \tag{A15}$$

Comparing boundary value problems (A7)–(A9) and (A13)–(A15), we see that they coincide if

$$\frac{\partial G(r;L)}{\partial L} = G(r;L)C(L),$$
$$\frac{\partial F(r;L)}{\partial L} = F(r;L)C(L), \tag{A16}$$

$$C(L) = -i\kappa(L) + \kappa^{-1}(L)\kappa'(L) - \kappa^{-1}(L)V^T \times (L)\kappa(L) + [V(L) + \kappa^{-1}(L)V^T(L)\kappa(L) - \kappa^{-1}(L)\kappa'(L)]G(L;L)/2.$$

Equalities (A16) can be considered linear differential embedding equations if they are supplemented with the appropriate original conditions

$$G(r;L)|_{L=r} = G(r;r),\ \ F(r;L)|_{L=r} = F(r;r) = i\kappa(r)[2E - G(r;r)],$$

and the matrix $G(L;\ L)$ is considered known for each fixed r. For this matrix, from the equality $\frac{dG(L;L)}{dL} = \left.\frac{\partial G(r;L)}{\partial r}\right|_{r=L} + \left.\frac{\partial G(r;L)}{\partial L}\right|_{r=L}$, and also using (A16), we have the matrix Riccati equation:

$$\frac{dG(L;L)}{dL} = 2i\kappa(L) - [ik(L) + V(L)]G(L;L) - G(L;L)[i\kappa(L) - \kappa^{-1}(L)\kappa'(L) + \kappa^{-1}(L)V^T(L)k(L)] + G(L;L) \times [V(L) + \kappa^{-1}(L)V^T(L)\kappa(L) - \kappa^{-1}(L)\kappa'(L)]G(L;L)/2, \tag{A17}$$

with the original condition $G(L_0;\ L_0) = E$, following from (A8), (A9) at $L \to L_0$. Thus, we have obtained embedding equations (A16), (A17) for finding the matrix $G(r;\ L)$ (and $F(r;\ L)$), after which, by calculating $\mathbf{G}(r) = G(r;L)\mathbf{b}(L)$, we obtain a solution to the boundary value problem for mode amplitudes (A4)–(A6). An essential circumstance in deriving the embedding equations is linearity of boundary value problem (A4)–(A6), as a result of which, when differentiating the equations with respect to parameter L, their structure does not change; therefore, relations (A16) are valid. To find the matrix $C(L)$, it remains only to find the derivative with respect to L in boundary condition (A11), as demonstrated in detail in (A14).

Equations (A16), (A17) and similar equations for the matrix $F(r;\ L)$ are completely equivalent (after transformation to vector form) to the original equations of the cross-sectional method for the wave zone of the source. Equation (A17) is the matrix Riccati equation describing the field in each section of an inhomogeneous medium when a mode of unit amplitude is incident this section. This field $G(L;\ L)$ is the sum of the incident and backscattered fields in each cross section: $G(L;\ L) = E + R(L;\ L)$. For the backscattered field $R(L;\ L)$, which we call the reflection (or scattering) coefficient of modes in an arbitrary cross section, it is easy to write the corresponding equation, which has a form similar to (A17), with the original condition $R(L_0;\ L_0) = \{0\}$ (zero matrix).

In most wave problems of acoustic signal propagation in inhomogeneous media, the backscattered field is neglected, and one passes to approximate methods of one-way propagation: the WKB method and the parabolic equation method [11–13]. In order to pass to one-way propagation of modes, in Eqs. (A16), it is necessary to set the reflection coefficients of the modes $R(L;\ L)$ equal to zero in each section of the medium, i.e., instead of the exact solution of Eq. (A17), set $G(r;r) = E$. Obviously (see the original condition for (A17) and condition (A3)), the last equality corresponds to free passage of a mode through an arbitrary section of the medium; thus, backscattering of modes is removed from consideration. Substituting the expression $G(L;L) = E$ into the formula for $C(L)$ leads to its simplification, and (A16) takes the form of expression (3) from Section 2 of this article. Thus, if the backscattered field is small (typical value of the reflection coefficient modulus $|R_m(L)|$ for significant modes in the problem under study is within 10^{-3}–10^{-2}), then it should be neglected, and the matrix Riccati equation should not solved. For modeling, one should use Eq. (A16), substituting into it the known functions $G(r;\ r)$, $C(r)$. The result is expression (3).

Note that matrix equation (A16) in one-way propagation approximation (3) allows for an exponential representation of the solution (in terms of a matrix exponent). This forms the basis for the statistical modeling in this article. For this, we pass from Eq. (A16) to the equation for transposed matrices, i.e.,

$$\frac{\partial G^T(r;L)}{\partial L} = C^T(L)G^T(r;L),\ \ G^T(r;r) = E,$$

and also perform the substitution $G^T(r;\ L) = \kappa^{-1/2}(r)\kappa^{1/2}(L)\tilde{G}(r;L)$ to remove from the equation the term with the derivative of the eigenvalue matrix $\kappa^{-1}(L)\kappa'(L)$. The solution to the resulting equation

$$\frac{\partial \tilde{G}(r;L)}{\partial L} = Q(L)\tilde{G}(r;L),\ \ \tilde{G}(r;r) = E,$$
$$Q(L) = -i\kappa(L) + \kappa^{-1/2}(L)\kappa^{1/2}(r) \times [V^T(L) - \kappa^{-1}(L)V(L)k(L)]\kappa^{1/2}(L)\kappa^{-1/2}(r)/2,$$

is represented by means of the matricant [39]:

$$(r;L) = P_r^L(Q) = E + \int_r^L Q(L)dL + \int_r^L Q(L)dL\int_r^L Q(\xi)d\xi + \dots$$

Obviously, in the considered one-way propagation approximation, the equations can be integrated both in terms of L for fixed r, and in terms of r for fixed L (with opposite sign). If at each step $\Delta r_k = r_{k+1} - r_k$ of the computational procedure $Q(r)$ approximates the constant matrix

$$Q(r) \cong \sum_{k=1}^{N-1} Q_k[\theta(r - r_k) - \theta(r - r_{k+1})],$$

where $\theta(r)$ is the unit function $\{\theta = 0$ for $r \le 0$, $\theta = 1$ for $r > 0\}$, then the matricant is represented by the product of the matrix exponentials [39]

$$\tilde{G}(r; L) \cong e^{Q_k \Delta r_k} \ldots e^{Q_2 \Delta r_2}\, e^{Q_1 \Delta r_1} E.$$

In model calculations, this makes it possible to simplify the numerical algorithm and increase the calculation speed. As well, to obtain the horizontal dependence of the mode amplitudes at each kth step of calculations, inverse transitions from matrices $\tilde{G}_k$ to matrices G_k^T, G_k and to the vector $\mathbf{G}_k$ of the mode amplitudes are carried out.

FUNDING

The study was carried out within the state assignment on the topic “Study of the Nature of Linear and Nonlinear Interaction of Geospheric Fields of Transition Zones of the World Ocean and Their Consequences”, state registration no. 124022100074-9.

CONFLICT OF INTEREST

The authors of this work declare that they have no conflicts of interest.

REFERENCES

1. M. A. Isakovich, Zh. Eksp. Teor. Fiz. **23**, 305 (1952).
2. V. V. Tamoikin and A. A. Fraiman, Izv. Vyssh. Uchebn. Zaved., Radiofiz. **11**, 56 (1968). https://doi.org/10.1007/BF01033538
3. Yu. A. Kravtsov, I. M. Fuks, and A. B. Shmelev, Izv. Vyssh. Uchebn. Zaved., Radiofiz. **14**, 854 (1971). https://doi.org/10.1007/BF01033177
4. F. G. Bass and M. Fuchs, *Wave Scattering from Statistically Rough Surfaces* (Nauka, Moscow, 1972; Pergamon, Oxford, 1979).
5. L. M. Brekhovskikh and Yu. P. Lysanov, *Theoretical Foundations of Ocean Acoustics* (Gidrometeoizdat, Leningrad, 1982) [in Russian].
6. J. A. Ogilvy, Rep. Prog. Phys. **50**, 1553 (1987).
7. M. Darmon, V. Dorval, and F. Baque, Appl. Sci. **10** (22), 8305 (2020). https://doi.org/10.3390/app10228305
8. A. N. Ivakin, J. Acoust. Soc. Am. **103**, 827 (1998).
9. A. N. Ivakin, J. Acoust. Soc. Am. **140**, 657 (2016). https://doi.org/10.1121/1.4959111
10. O. E. Gulin, Sov. Phys. Acoust. **30** (4), 276 (1984).
11. L. M. Brekhovskikh and O. A. Godin, in *Acoustics of Inhomogeneous Media* (Nauka, Moscow, 2009), **Vol. 2** [in Russian].
12. F. B. Jensen, W. A. Kuperman, M. B. Porter, and H. Schmidt, *Computational Ocean Acoustics* (Springer, New York, Dordrecht, Heildelberg, London, 2011).
13. M. D. Collins, J. Acoust. Soc. Am. **94**, 2269 (1993).
14. W. A. Kuperman and H. Schmidt, J. Acoust. Soc. Am. **79**, 1767 (1986).
15. B. H. Tracey and H. Schmidt, IEEE J. Ocean. Eng. **22** (2), 317 (1997).
16. S. A. Stotts, D. P. Knobles, and R. A. Koch, J. Acoust. Soc. Am. **129** (5), EL172 (2011).
17. D. P. Knobles, S. A. Stotts, and R. A. Koch, J. Acoust. Soc. Am. **113**, 781 (2003).
18. I. O. Yaroshchuk and O. E. Gulin, *Statistical Modelling for Hydroacoustical Problems* (Dal’nauka, Vladivostok, 2002) [in Russian].
19. O. E. Gulin and I. O. Yaroshchuk, J. Comput. Acoust. **22**, 1440002 (2014). https://doi.org/10.1142/S0218396X14400025
20. O. E. Gulin and I. O. Yaroshchuk, J. Comput. Acoust. **22**, 1440006 (2014). https://doi.org/10.1142/S0218396X14400062
21. F. Zhu, O. E. Gulin, and I. O. Yaroshchuk, Appl. Sci. **9** (9), 1841 (2019). https://doi.org/10.3390/app9091841
22. O. E. Gulin and I. O. Yaroshchuk, Acoust. Phys. **63** (2), 168 (2017). https://doi.org/10.1134/S1063771017020051
23. O. E. Gulin and I. O. Yaroshchuk, J. Mar. Sci. Eng. **10** (6), 822 (2022). https://doi.org/10.3390/jmse10060822
24. O. E. Gulin and I. O. Yaroshchuk, Acoust. Phys. **64** (2), 186 (2018). https://doi.org/10.1134/S1063771018020069
25. F. Zhu, O. E. Gulin, and I. O. Yaroshchuk, Appl. Sci. **11** (23), 11575 (2021). https://doi.org/10.3390/app112311575
26. O. E. Gulin, Acoust. Phys. **52** (1), 17 (2006).
27. O. E. Gulin, Acoust. Phys. **52** (1), 17 (2006). https://doi.org/10.1134/S1063771006010039
28. O. E. Gulin, Acoust. Phys. **54** (4), 495 (2008). https://doi.org/10.1134/S106377100804009X
29. O. E. Gulin, Acoust. Phys. **56** (5), 684 (2010). https://doi.org/10.1134/S1063771010050143
30. O. E. Gulin, Acoust. Phys. **56** (5), 613 (2010). https://doi.org/10.1134/S1063771010050027
31. X. Tang, F. D. Tappert, and D. B. Creamer, J. Acoust. Soc. Am. **120** (6), 3539 (2006). https://doi.org/10.1121/1.2372446
32. D. S. Yashin and B. I. Kim, Geol. Nefti Gaza **4**, 25 (2007).

33. V. A. Grigor'ev, V. G. Petnikov, A. G. Roslyakov, and Ya. E. Terekhina, Acoust. Phys. **64** (3), 331 (2018). https://doi.org/10.1134/S1063771018030053

34. V. A. Grigor'ev and V. G. Petnikov, Acoust. Phys. **62** (6), 700 (2016). https://doi.org/10.1134/S1063771016050031

35. M. D. Collins and E. K. Westwood, J. Acoust. Soc. Am. **89** (3), 1068 (1991).

36. S. M. Rytov, Yu. A. Kravtsov, and V. I. Tatarskii, *Foundations of Statistical Radiophysics,* Vol. 2: *Random Fields* (Nauka, Moscow, 1978) [in Russian].

37. V. I. Klyatskin, *Immersion Method for Waves Propagation Theory* (Nauka, Moscow, 1986) [in Russian].

38. V. I. Klyatskin, *Stochastic Equations from the Physicist Point of View* (Fizmatlit, Moscow, 2001) [in Russian].

39. F. R. Gantmakher, *Matrix Theory* (Fizmatlit, Moscow, 1988) [in Russian].